Power Electronic Systems
Laboratory

© 2014 IEEE

IEEE Transactions on Industrial Electronics, Vol. 61, No. 6, pp. 3089-3098, June 2014

An Active Magnetic Damper Concept for Stabilization of Gas Bearings in High-Speed Permanent-Magnet Machines

A. Looser,
J. W. Kolar

This material is published in order to provide access to research results of the Power Electronic Systems Laboratory / D-ITET / ETH Zurich. Internal or personal use of this material is permitted. However, permission to reprint/republish this material for advertising or promotional purposes or for creating new collective works for resale or redistribution must be obtained from the copyright holder. By choosing to view this document, you agree to all provisions of the copyright laws protecting it.

Eidgenössische Technische Hochschule Zürich
Swiss Federal Institute of Technology Zurich

An Active Magnetic Damper Concept for Stabilization of Gas Bearings in High-Speed Permanent-Magnet Machines

Andreas Looser, *Student Member, IEEE*, and Johann W. Kolar, *Fellow, IEEE*

***Abstract*—The successful application of ultrahigh-speed electrical-drive systems in industrial products is currently limited by lacking high-speed bearing technologies permitting high reliability and long lifetime. Promising bearing technologies for high rotational speeds are contactless bearing concepts such as active magnetic bearings or gas bearings. While magnetic bearings usually are major electromechanical systems with substantial complexity, gas bearings allow compact realizations with high load capacity and stiffness; however, poor dynamic stability has been limiting their use at high rotational speeds. Following a hybrid bearing approach with an aerodynamic gas bearing for load support, a small-sized active magnetic damper concept is proposed to enable the stable high-speed operation of the gas bearing with a minimum of additional complexity and costs. As for the effective stabilization of the gas bearing, a high-quality displacement measurement is essential, and a new eddy-current-based rotor-displacement self-sensing concept employing an auxiliary signal injection and rotor displacement measurement circuit is presented. A hardware implementation of the proposed concept is shown providing high-resolution measurement signals.**

***Index Terms*—Active magnetic damper, high-speed permanent-magnet machines, signal injection self-sensing, vibration control.**

I. Introduction

FUTURE ultrahigh-speed electrical drives are expected in emerging applications such as turbocompressor systems for fuel cells and heat pumps, generators for portable gas or air turbines, printed circuit board (PCB) drilling, machining spindles, and optical devices [1], [2]. Rotational speeds for these applications range from 200 kr/min to 1 Mr/min at power ratings of a few tens of watts to a few kilowatts. The main challenges and limitations involved with high-speed machine design which are of thermal, elastic, and rotordynamical nature have been discussed in [3]. Thus, a multiphysical machine optimization has been performed in [4] for the design of a 200-kr/min 2-kW permanent-magnet machine. An optimized machine design with low losses at high speeds as well as a robust mechanical rotor construction in order to cope with rotordynamics and the high stresses at high rotational speeds has been presented in [5], and the operation of a 100-W permanent-magnet machine has been demonstrated at speeds up to 1 Mr/min [1]. However, the use of such ultrahigh-speed drive systems in industrial applications is limited mainly due to the absence of reliable bearings with long lifetime at high rotational speeds. Precision ball bearings designed for dental drills with a maximum rated speed of 400 kr/min (corresponding to a DN number of 1.5 million)[1] showed a total lifetime of around 200–300 h in cyclic tests where the speed was varied between 200 and 500 kr/min. However, for future industrial high-speed applications, a lifetime of several years at speeds beyond 500 kr/min would be required.

Promising candidates for high-speed bearings with longer lifetimes are contactless concepts such as active magnetic bearings or gas bearings, where, for the latter, the rotor is carried by the fluid film generated between the bearing bushing and the journal.

For active magnetic bearings, very high speed operation has been demonstrated with a self-bearing permanent-magnet motor design at rotational speed of up to 400 kr/min [6], which in recent achievements could be further increased to 505 kr/min [7]. Aside from the possibility for high-speed operation, one of the main benefits of active magnetic bearings is also their capability of active vibration control of structural resonance [8], which can allow operation at speeds beyond the rotor's natural frequencies. However, employing active magnetic bearings usually increases the drive system complexity due to the additional actuators, sensors, power amplifiers, and control and often yields less compact drive systems, particularly for drive systems of small rated power.

Gas bearings exist as aerostatic and aerodynamic bearings. For the aerostatic bearing, the rotor is carried by the fluid film generated by an external pressurized air supply. For aerodynamic bearings, the fluid film is generated by the journal rotation itself, therewith eliminating the need of an external pressurized air supply and allowing for a very compact design. As illustrated in Fig. 1 for the case of a plain journal bearing, a pressure is generated when the journal is displaced by ε. Under rotation, the fluid is dragged into the formed converging gap, generating a high pressure. On the diverging side, a lower pressure occurs. As a result, a net force acts on the journal, restoring the journal to its centered position. Compared to magnetic bearings, gas bearings can usually be designed much

Manuscript received January 31, 2013; revised April 25, 2013 and July 25, 2013; accepted August 18, 2013. Date of publication October 1, 2013; date of current version December 20, 2013.

The authors are with Power Electronic Systems Laboratory, ETH Zurich, 8092 Zurich, Switzerland (e-mail: looser@lem.ee.ethz.ch; kolar@lem.ee.ethz.ch).

Color versions of one or more of the figures in this paper are available online at http://ieeexplore.ieee.org.

Digital Object Identifier 10.1109/TIE.2013.2284152

[1]The DN number is defined as the bearing diameter (D) in millimeters times the rotational speed (N) in revolutions per minute.

0278-0046 © 2013 IEEE

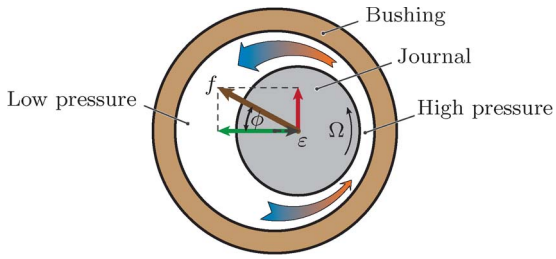

Fig. 1. Working principle of a gas-lubricated plain journal bearing: Due to the formation of a converging air gap when the journal is displaced, the air is dragged into the converging gap, generating a pressure distribution which results in a force restoring the journal to its centered position.

smaller for the same load capacity and stiffness, for which reason more compact drive systems can be realized.

One of the major challenges with high-speed gas bearings, however, is the self-excited whirl instability which limits the maximum operating speed. The phenomenon of whirl instability has been known from the beginning of fluid film lubrication and has been thoroughly studied, e.g., in [9]. Usually, the bearing restoring force encloses an angle ϕ to the displacement vector ε, which is known as the bearing's attitude angle. Thus, the main causes for the instability are the destabilizing azimuthal force component perpendicular to the journal displacement, instead of a purely radial force into the bearing center (as visualized in Fig. 1), combined with relatively low damping from the fluid film itself. In order to cope with the gas bearing's instability encountered at higher speeds or with heavier rotors, a variety of gas-bearing types have been developed in the history of fluid film lubrication. Gas-bearing types known for their relatively good stability are, e.g., the tilting-pad bearing [10], the herringbone-grooved bearing [11], and also the foil bearings. For foil bearings, speeds of up to 700 kr/min have been reported, however driven by a relatively light air turbine [12]. Foil bearings supporting the rotor of a permanent-magnet brushless dc machine at a speed of 350 kr/min are reported in [13].

A further increase of rotational speed up to 1.2 Mr/min has been achieved with a helium-driven turbine employing a flexible supported bearing bushing and an oil damper [14]. However, with the elastic support, also the overall stiffness of the bearing-damper assembly is reduced. In [15], the concept of the damped elastic support has been applied to a permanent-magnet synchronous machine, and a speed of 410 kr/min has been achieved; in order to increase the speed to the targeted 600 kr/min, a further increase in accuracy for rotor fabrication is suggested.

Another approach to stabilize fluid film bearings is encountered, e.g., in [16] where active magnetic bearings are used for vibration control. Although increasing the size and complexity of the drive system, the active magnetic bearings are effectively used to control the oil whirl and oil whip instability of a journal bearing, therewith increasing the range of operation.

It can be summarized that, generally, there have been two strategies to improve the gas bearing's stability. Improvements have been achieved either by a reduction of the destabilizing azimuthal force component usually accomplished by a special bearing geometry and/or by the introduction of additional damping from outside the fluid film.

In a given application, the bearings need to support a rotor of an electrical machine capable of providing a required shaft power. The rotor of such a system will be heavier than the air turbines used for record speed bearing tests, and therefore, instability occurs already at lower speeds as the aforementioned examples with permanent-magnet rotors show. A stable design for, e.g., a herringbone-grooved journal bearing supporting a relatively heavy permanent-magnet rotor would theoretically be possible by scaling down the gas-bearing clearance. However, this approach is hardly feasible because of the requirement for high precision fabrication with very tight production tolerances which finally would limit an industrial implementation. Unfortunately, gas-bearing designs with more relaxed production tolerances would become unstable already at lower speeds for many of the targeted permanent-magnet machine applications.

Therefore, a hybrid bearing concept employing a self-sensing active magnetic damper (AMD) was proposed by the authors in [17], intended to enable stable operation at high speeds also for heavy permanent-magnet rotors. The hybrid concept combines the advantages of high load capacity and stiffness of the gas bearing with the capability of vibration control of the active magnetic damper and allows for a feasible gas-bearing design which, without active control, would become unstable at high speeds. With the proposed concept, no decrease of overall stiffness and load capacity has to be traded for better stability as is the case with the concept of a damped elastic support. Furthermore, the increase of complexity added by the active magnetic damper is kept at a minimum due to the absence of additional sensors, i.e., due to the self-sensing approach; the absence of additional sensors allows to keep the rotor length as short as possible, which is a key factor in high-speed machine design. With the damper only providing vibration control and not the full rotor support, the damper can be designed very small.

In this paper, the original conceptual work is advanced with an implementation of the proposed self-sensing topology on a PCB and measurements thereof. Moreover, a new flexible printed circuit (FPC) winding is presented, replacing the wire-wound conventional air-gap winding and allowing for an even more compact damper design which then enables a more efficient motor design.

First, the hybrid bearing concept, including motor, gas bearings, and magnetic damper, is explained in Section II. The rotor displacement self-sensing method employing an eddy-current-based high frequency signal injection approach is described in Section III. The hardware implementation of the self-sensing circuit together with the FPC winding is presented in Section IV, where, also, measurement results for the radial rotor displacement self-sensing in a prototype permanent-magnet machine are shown.

II. Hybrid Bearing Concept

A conceptual drawing of a high-speed permanent-magnet machine with the proposed hybrid bearing approach is shown in Fig. 2. The electrical motor is a slotless-type permanent-magnet synchronous machine constructed according to the machine design in [5], which has been well proven for high rotational speeds. The rotor consist of a diametrically magnetized

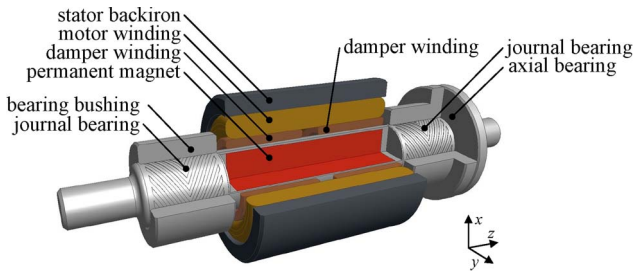

Fig. 2. Conceptual drawing of a high-speed permanent-magnet machine with a hybrid bearing concept employing gas bearings in combination with active magnetic dampers.

permanent magnet encased in a retaining sleeve to protect the brittle permanent magnet from breaking due to the high centrifugal forces at high speeds. For the motor winding, slotless-type air-gap windings with litz wire are used in order to minimize the eddy-current losses caused by the permanent-magnet field at high frequencies. For the same reason, the stator back iron consists of amorphous iron. More information on the conceptual design of high-speed slotless permanent-magnet machines is found in [1], [5], and [18].

The gas bearings are located outside the motor's active region. A restriction to the type of journal gas bearing is not *a priori* given. In order to minimize the amount of required damping, a gas bearing with improved performance at high speeds is favored, such as the gas-bearing types discussed in Section I. For manufacturing reasons, a bearing type with a fixed geometry (i.e., without foils or moving parts) is preferred, e.g., the herringbone-grooved journal bearing depicted in Fig. 2. The axial bearing can be a spiral grooved or Rayleigh-step bearing, as commonly used in gas-bearing systems. For axial bearings, unstable behavior is much less of a concern than for journal bearings. Therefore, no magnetic dampers are required for axial stabilization.

Two active magnetic bearing concepts are known for the realization of the magnetic damper, namely, the homopolar and the heteropolar concept. The term heteropolar refers to a configuration where the rotor is exposed to a magnetic field with alternating polarity as it rotates, and the term homopolar denotes a configuration with unchanging polarity [19]. Generally, both a homopolar and a heteropolar damper topology would be suited for vibration control of a shaft rotating at high speeds.

The heteropolar damper concept requires a diametrically magnetized permanent magnet which is already existing and needed for drive torque generation. Hence, integration into the active region of the motor is straightforward with an additional air-gap winding for the damper and yields a very compact design [6]. Clearly, by integrating the damper into the active region of the motor, the torque capability of the machine is reduced. A damper design of minimal wall thickness is therefore advantageous.

A homopolar damper realization would require additional axially magnetized permanent magnets; this complicates the rotor construction for which reason the homopolar concept is not further considered.

The force generation principle of the heteropolar damper design is visualized in Fig. 3. The inner winding (damper winding) is used to produce a fundamental current distribution with a pole-pair number of two; hence, with the magnetic field of the diametrically magnetized permanent magnet, Lorentz forces act on the winding, respectively, and a resultant reaction force is obtained on the rotor. The outer winding (motor winding) with only one pole pair produces a force couple, and therefore, a torque results on the rotor.

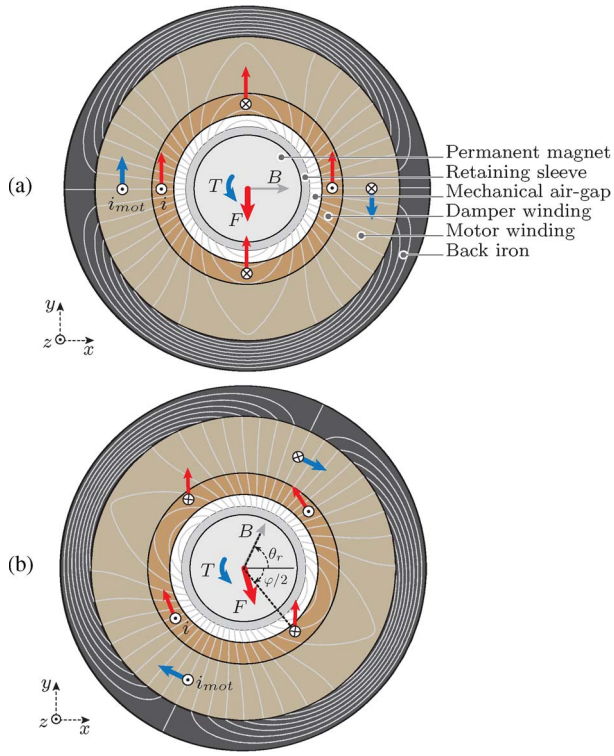

Fig. 3. Force generation by means of a two-pole-pair winding for the magnetic damper winding arranged on the inner diameter of the motor winding. (a) Situation with a rotor angle of $\theta_r = 0$ and an AMD current space vector phase angle of $\varphi = 0$. (b) Situation with arbitrary angles θ_r and φ.

The damper forces in the two radial directions x and y can be described as

$$f_x = K_I \cdot i_d \tag{1}$$

$$f_y = K_I \cdot i_q \tag{2}$$

where K_I is the force-current constant of the damper and i_d and i_q are the rotor flux-oriented stator currents in dq coordinates. Note that K_I is the direction independent for the present machine design with a diametrically magnetized permanent magnet. The rotating dq-coordinate system is defined by the rotor angle θ_r, which is given by the direction of the permanent-magnet flux. Accordingly, the flux-oriented currents can be defined as

$$i_d = -\hat{I}\sin(\varphi - \theta_r) \tag{3}$$

$$i_q = \hat{I}\cos(\varphi - \theta_r) \tag{4}$$

where $\hat{I}$ and φ denote the AMD current space vector's amplitude and phase angle, respectively.

In Fig. 3(a), the situation of a pure q current is drawn, resulting in a force in the y-direction. Rotating the current distribution by -45° corresponds to a pure d current distribution,

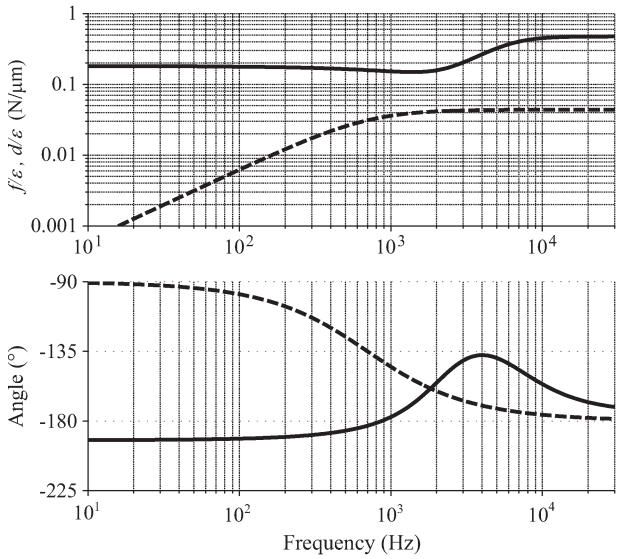

Fig. 4. Bode diagram of (solid line) the dynamic stiffness (f/ε) and its phase angle for the gas bearing and (dashed line) the damping force (d/ε) provided by the magnetic damper, which is needed to stabilize the rotor in the unstable region around 300 kr/min.

resulting in a force in the x-direction. The situation for arbitrary rotor and current space vector angles is depicted in Fig. 3(b).

In the simplest case, vibration control is accomplished by generating damper forces proportional to the rotor's radial velocities. Based on the velocity in the according directions

$$v_x = \frac{d}{dt}\varepsilon_x \tag{5}$$

$$v_y = \frac{d}{dt}\varepsilon_y \tag{6}$$

expressed in terms of the rotor displacements ε_x and ε_y, the damping control reference currents are given by

$$i_d^* = -\frac{d}{K_I} \cdot v_x \tag{7}$$

$$i_q^* = -\frac{d}{K_I} \cdot v_y \tag{8}$$

where d is the damping factor. For vibrations with high frequencies, the aforementioned time derivative would yield very high damper currents. Therefore, a first-order low-pass filter is applied, limiting damping at higher frequencies.

Considering the example of a herringbone-type bearing with a diameter of 6 mm, a length of 8 mm, a clearance of 15 μm, and curved grooves, optimized for maximum stability at 500 kr/min, the highest amount of damping force occurs at speeds around 300 kr/min. For this operating point, the dynamic stiffness of the gas bearing (bearing reaction force per displacement, f/ε) has been calculated using a finite difference method to solve the partial differential equation for the bearing clearance average pressure, which is based on the narrow groove theory originally proposed in [20]. Based on a rotor dynamic analysis incorporating the calculated dynamic bearing stiffness, the required damping force needed for stabilization can be determined. The calculated damper force as well as the dynamic stiffness of the gas bearing is plotted in the Bode diagram in Fig. 4. Compared

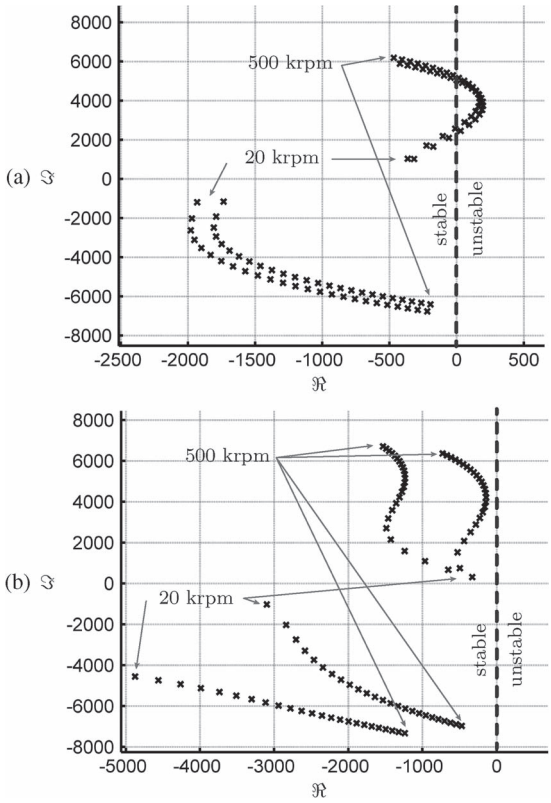

Fig. 5. Speed-dependent root loci of the bearing-rotor system. (a) Unstable system without active magnetic stabilization. (b) Stable system with active magnetic stabilization.

to the force provided by the gas bearing, the required damping force is relatively small. As a result, the magnetic dampers can be designed significantly smaller compared to a drive system with magnetic bearings providing the full rotor support.

The speed-dependent root loci of the rotor-bearing system without active stabilization are depicted in Fig. 5(a). With increasing speed, the poles move toward the imaginary axis and become unstable at a speed of around 80 kr/min. Fig. 5(b) shows the root loci of the system employing active magnetic damping. The system is stabilized for all speeds, and accordingly, all unstable poles have shifted into the left half of the imaginary plane.

In order to produce damping forces in response to radial rotor motion, an accurate radial rotor velocity measurement is needed. As the velocity can be easily obtained with the time derivative of the displacement, a rotor displacement measurement could also be used. Rotor radial displacements or velocities to be measured are expected on the order of 0.1–10 μm and 1–100 mm/s, respectively. With AMBs, the radial clearance is usually on the order of some hundreds of micrometers while the clearance of the gas bearings will be maximally 10 or 20 μm. Hence, the sensitivity and resolution requirements of the rotor displacement measurement are expected to be much higher compared to the requirements for state-of-the-art AMBs. Achieving high sensitivity and accuracy of the velocity or displacement measurement is therefore considered as one of the main challenges implicated by the proposed hybrid bearing concept.

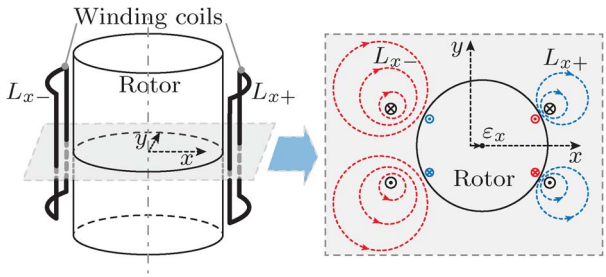

Fig. 6. Eddy-current displacement measurement employing two oppositely arranged search coils.

III. Displacement Measurement—Eddy-Current Self-Sensing

Commonly used approaches for rotor displacement measurement in self-sensing magnetic bearings are based on the observation of the actuator's inductance which is a function of the magnetic air gap and hence also of the rotor displacement. Therewith, the bearing linear power amplifier or switched amplifier is used to modulate the bearing current or superimpose a test signal in order to observe the displacement-dependent self- or mutual-inductance change [21]–[23]. In order to observe an inductance change caused by a displaced rotor, ferromagnetic materials on the rotor are required, which, however, is not the case for the present machine. Therefore, no change of the inductance occurs, and the method cannot be applied.

In conventional active magnetic bearing systems, eddy-current sensors have been commonly used and have been well proven [24]. Furthermore, they are not restricted to only ferromagnetic materials and have shown very high sensitivity. Therefore, eddy-current-based position sensing seems promising.

For the present magnetic damper, a concept is proposed, where the damper coils, which are implemented as air-gap windings, are simultaneously used as eddy-current displacement sensors. With the twofold use of the damper winding, i.e., a winding in a self-sensing configuration, no additional rotor length is required for position sensing. To obtain the high sensitivity of the eddy-current displacement measurement, the injection of a test signal with a frequency of up to 10 MHz is required. Signal injection at such a high frequency cannot be easy accomplished by a linear or switched power amplifier used for the damper current; thus, an auxiliary signal injection and measurement circuit is required. Although the term self-sensing does not apply to the full system as auxiliary circuits are needed on the electronic side, it applies fully to the machine part which can be realized in smaller size due to reduced part count. Therefore, the denotation is continued in the following.

For the measurement in the x-direction, a coil pair with coils denoted as L_{x+} and L_{x-} is required, as depicted in Fig. 6. When the rotor is displaced by a positive value of ε_x, the impedance of L_{x+} decreases due to eddy currents on the approaching rotor. Accordingly, the impedance of L_{x-} increases. For the measurement in the y-direction, another coil pair with coils denoted as L_{y+} and L_{y-} is required. Thus, in order to measure the displacement of the rotor in the two radial directions x and y, a damper winding with two pairs of oppositely arranged coils could be employed, as illustrated in Fig. 7.

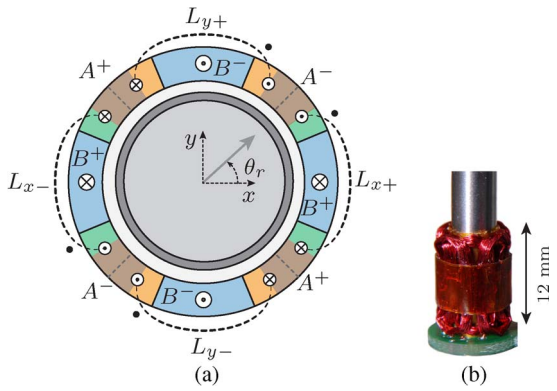

Fig. 7. (a) Winding scheme of the two-phase magnetic damper winding with oppositely arranged coil pairs for eddy-current-based high frequency signal injection displacement sensing. The dots designate the winding sense of the coils. (b) Wire-wound prototype winding.

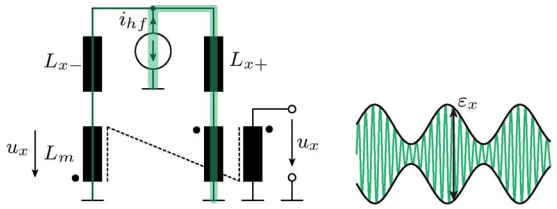

Fig. 8. Bridge-connected windings L_{x+} and L_{x-} for the measurement of the displacement-dependent impedance change using differentially coupled inductors. The high frequency injected current i_{hf} splits according to the instantaneous impedance value of the coils L_{x+} and L_{x-}, yielding modulated measurement signal u_x with an amplitude proportional to the rotor displacement ε_x.

All four coils L_{x+}, L_{x-}, L_{y+}, and L_{y-} connected in series form the first phase of the damper winding, denoted as phase A. The order of the series connection is chosen later in order to meet the requirements for the intended signal injection self-sensing technique. To form a damper winding with a pole-pair number of $p = 2$ and $m = 2$ phases, another set of series-connected coils is required for the second phase B, with its conductors arranged 45° from the conductors of phase A. Phase B is preferably implemented as an ordinary series connection of the winding turns denoted as L_B; no additional tappings are required within phase B.

For the derivation of the displacement measurement principle, the impedance of the coil L_{x-} is assumed a general function $Z_{x-} = Z_x(\varepsilon_x, \varepsilon_y)$ of the rotor displacements ε_x and ε_y. Assuming symmetry, L_{x+} corresponds to $Z_{x+} = Z_x(-\varepsilon_x, \varepsilon_y)$. For very small rotor displacements, the coil impedances can then be described by their first-order approximations as

$$Z_{x+} \approx Z_0 - \frac{\partial Z_x}{\partial \varepsilon_x} \cdot \varepsilon_x + \frac{\partial Z_x}{\partial \varepsilon_y} \cdot \varepsilon_y \tag{9}$$

$$Z_{x-} \approx Z_0 + \frac{\partial Z_x}{\partial \varepsilon_x} \cdot \varepsilon_x + \frac{\partial Z_x}{\partial \varepsilon_y} \cdot \varepsilon_y \tag{10}$$

where $Z_0 = Z_x(0, 0)$ denotes the coil impedance for a perfectly centered rotor. To measure the impedance change, a measurement bridge as depicted in Fig. 8 is proposed. No differential voltage measurement is needed as would be the case with a conventional Wheatstone bridge. Instead, the common

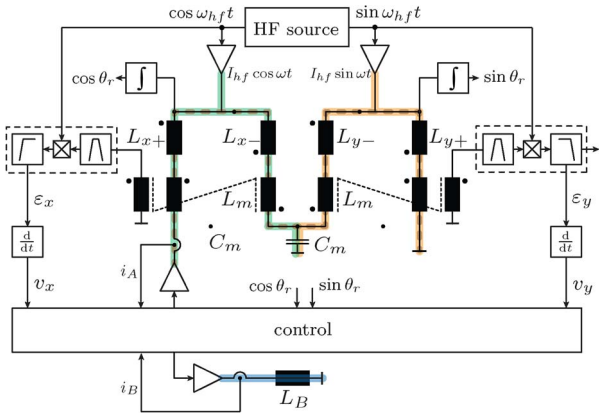

Fig. 9. Self-sensing high frequency signal injection circuit for displacement measurement in x- and y-directions (ε_x and ε_y) with power amplifiers and control. Actuator currents (brown and blue for phase A and phase B) and high frequency injected currents (green and orange) are colored according to the AMD winding scheme of Fig. 7.

mode voltage is canceled with the use of differentially coupled inductors L_m.

Assuming ideal inductors L_m without a parasitic series resistance, the voltage across the inductor measured to ground is given by

$$u_x = i_{hf} \cdot \frac{Z_m}{Z_0 + \frac{\partial Z_x}{\partial \varepsilon_y} \cdot \varepsilon_y + 2Z_m} \cdot \frac{\partial Z_x}{\partial \varepsilon_x} \cdot \varepsilon_x \tag{11}$$

where i_{hf} denotes the current injected by a high frequency current source. Assuming that the impedance change $(\partial Z_x/\partial \varepsilon_y) \cdot \varepsilon_y$ due to a displacement in the y-direction is small compared to the nominal coil impedance Z_0, the measured voltage simplifies to

$$u_x = i_{hf} \cdot \frac{Z_m}{Z_0 + 2Z_m} \cdot \frac{\partial Z_x}{\partial \varepsilon_x} \cdot \varepsilon_x \tag{12}$$

and is directly proportional to the displacement ε_x. If a parasitic series resistance of L_m is present, an offset voltage would occur for which reason the voltage u_x is better measured on the terminals of the third coupled winding as indicated in Fig. 8.

Fig. 9 shows a possible combination of the measurement bridge and the required series connection of the winding coils of phase A. In order to obtain position information in both radial directions x and y, high frequency test signals need to be injected. As the two coil pairs for position measurement in the x- and y-directions are magnetically coupled, orthogonal injection signals are needed to avoid a coupling of the two measurement channels. Hence, e.g., a sine and a cosine or 90° shifted rectangular signals can be used for signal injection. The high frequency currents denoted as $I_{hf} \cos \omega t$ and $I_{hf} \sin \omega t$ are injected capacitively through C_{in}, which is necessary for two reasons. First, the damper current from the power amplifier is not supposed to be influenced at low frequencies, and second, the signal-injecting buffers need to be decoupled from the midpoint of the windings which otherwise would expose the buffers to the high back-electromotive force (back-EMF) voltage at high rotational speeds. A further additional capacitor C_m is added which represents a short circuit for the high frequency signal. The output of the power amplifier

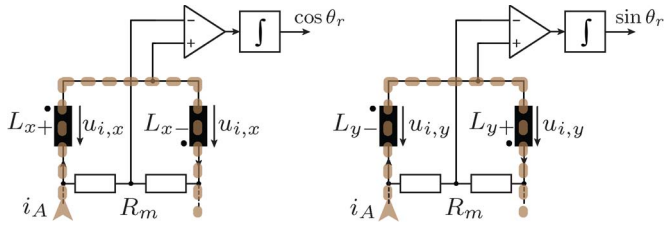

Fig. 10. Back-EMF-based angular rotor position measurement with compensation of resistive and inductive voltage contributions due to the AMD actuator current i_A. The back-EMF voltages are indicated as $u_{i,x}$ and $u_{i,y}$, respectively.

for phase A needs to exhibit low impedance to ground at high frequencies whereby, together with C_m, the measurement bridge is obtained. A low output impedance of the power amplifier can be accomplished by connecting an LC filter to its output stage. The capacitor C_m has to be dimensioned not to affect the damper current from the power amplifier at low frequencies. Given an injection frequency of 10 MHz and assuming a damper control bandwidth of less than 10 kHz, the impedance of C_m at these frequencies differs at least by 60 dB; hence, signal separation can be easily guaranteed.

In order to obtain the displacements, the known steps for the demodulation of an amplitude-modulated signal are followed. First, the signals u_x and u_y are fed through a bandpass filter followed by a frequency mixer. After the mixer, the signals are processed through a low-pass filter which eliminates the high frequency spectral components and yields a signal proportional to the displacements ε_x and ε_y. The displacement signals are then further processed to obtain the radial velocities needed for the control of the damper currents.

In order to transform the damper reference currents from the rotating dq-coordinate system of the rotor into winding reference currents according to

$$i_A^* = i_d^* \cos \theta_r - i_q^* \sin \theta_r \tag{13}$$

$$i_B^* = i_d^* \sin \theta_r + i_q^* \cos \theta_r \tag{14}$$

also the angular rotor position θ_r needs to be provided. Therefore, the back-EMF voltage is measured at the winding midpoint tapping. According to Luomi *et al.* [5], the radial component of the magnetic field density in the air gap of a slotless machine with a diametrically magnetized permanent magnet is $B_r \propto cos(\theta_r)$. Therefore, the induced voltages $u_{i,x}$ and $u_{i,y}$ over the coils L_x and L_y must be proportional to $u_{i,x} \propto \dot{\theta}_r \cdot \cos \theta_r$ and $u_{i,y} \propto \dot{\theta}_r \cdot \sin \theta_r$. The integration of the back EMF yields again proportionality to the permanent-magnet flux and, hence, signals proportional to $\cos \theta_r$ and $\sin \theta_r$ which can be used directly for the aforementioned transformation.

In Fig. 9, the back-EMF-based angular position measurement is indicated by a simple voltage measurement and the subsequent integrator block. Aside from the back-EMF voltage, also resistive and inductive voltages occur across the winding coils due to the AMD actuator current i_A. Thus, in order to cancel out these unwanted voltage contributions in the measurement, the voltage is measured relative to a reference potential generated by means of a resistive voltage divider R_m as depicted in Fig. 10.

TABLE I
DAMPER WINDING SPECIFICATIONS

Wire-wound winding	
Inner diameter	6.5 mm
Outer diameter	8.5 mm
Length	12.0 mm
Number of turns (per coil side)	20
Inductance phase A (10 kHz)	4×5.6 μH
Inductance phase B (10 kHz)	25 μH
Resistance phase A	4×1.2 Ω
Resistance phase B	4.6 Ω
Force-current constant K_I	0.46 N/A
Flexible printed circuit (FPC) winding	
Inner diameter	6.5 mm
Outer diameter	7.4 mm
Length	9.5 mm
Number of turns (per coil)	18
Inductance phase A (10 kHz)	4×2.6 μH
Inductance phase B (10 kHz)	11.6μH
Resistance phase A	$4 \times 3.5\Omega$
Resistance phase B	9.0Ω
Force-current constant K_I	0.3 N/A

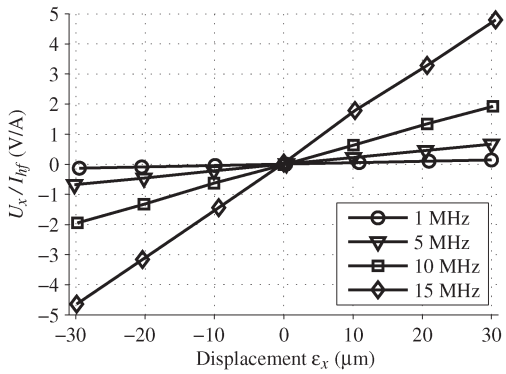

Fig. 11. Measurement bridge output voltage U_x normalized with the injected current I_{hf} as a function of the rotor displacement ε_x.

IV. HARDWARE IMPLEMENTATION AND MEASUREMENTS

In the preliminary work [17], a wire-wound air-gap winding [see Fig. 7(b)] and sensitivity measurements thereof were presented showing the feasibility of the proposed self-sensing approach. For the sensitivity measurement, a 6-mm stainless steel rod in place of the rotor and a wire-wound winding as specified in Table I are used. The winding is connected in a measurement bridge according to Fig. 8. A high frequency current with an amplitude of $I_{hf} = 20$ mA is injected into the winding, and the voltage U_x is measured at the measurement bridge output. For the coupled inductor L_m, a double-aperture core (Epcos K1) with an inductance of 3×10 μH is used. Fig. 11 shows the measured output voltage U_x normalized with the injected current I_{hf} as a function of the rotor displacement ε_x for various frequencies. If the voltage U_{hf} is also measured, the relative impedance change of the winding can be determined as

$$\frac{\Delta Z_x}{Z_0} = \frac{U_x(I_{hf}Z_m + U_{hf})}{U_x^2 + I_{hf}Z_m U_{hf}}. \tag{15}$$

The obtained impedance change as a function of the rotor displacement ε_x is plotted in Fig. 12. At a frequency of 10 MHz,

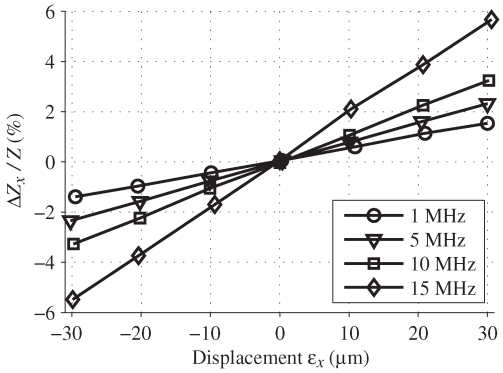

Fig. 12. Impedance change ΔZ_x of a damper winding coil related to its total impedance Z as a function of the rotor displacement ε_x.

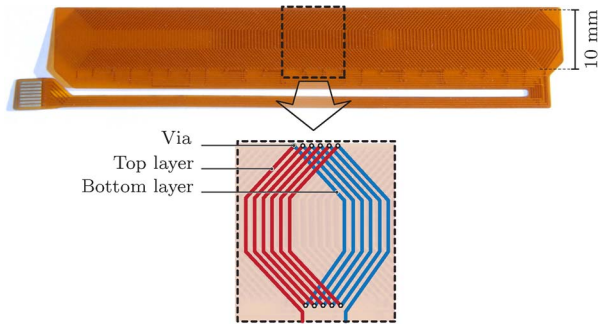

Fig. 13. Prototype active magnetic damper winding implemented as two-layer FPC.

the relative impedance change is approximately 0.1% per micrometer which is over 100 times more than for the eddy-current sensor for AMBs analyzed in [25] which uses printed windings on a rigid-type multilayer PCB arranged perpendicular to the rotor. The higher sensitivity mainly originates from the different arrangement of the coils which are located at a closer distance to the rotor. Furthermore, due to the self-sensing approach, the proposed concept profits from exploiting a larger portion of the rotor area for position sensing which is inaccessible with state-of-the-art eddy-current sensor types.

In this paper, the wire-wound winding is replaced, and a damper winding implemented as a two-layer FPC is proposed which allows for a more compact motor design. The FPC winding is made from a 25-μm polyimide substrate with 35-μm-thick base copper on both sides. Together with the coverlays, a total thickness of 0.15 mm is obtained. A picture of the prototype is shown in Fig. 13. The specifications of the winding are given in Table I.

Like the wire-wound winding, the FPC winding contains two oppositely arranged coil pairs for displacement sensing combined into a phase A and another set of coils combined to form a phase B. The FPC is rolled three times to obtain the final damper winding. The individual coils are realized in a rhombic shape as considered in [26] for FPC windings for brushless dc machines.

A single winding turn consist of a copper trace on the top layer as well as of a trace on the bottom layer; hence, two via connections are needed for each turn. The via bore and pad

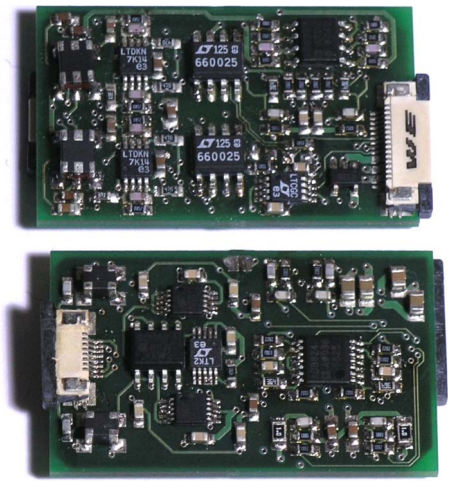

Fig. 14. Prototype PCB implementation of the proposed self-sensing circuit, top and bottom views. Dimensions: $22.5 \times 38 \times 6.5$ mm^3.

diameters were constrained to 100 and 300 μm, respectively, for manufacturing effort and cost reasons. In order to minimize the dc winding resistance, the copper trace width should be chosen maximal and hence equal to the via-pad diameter. However, with such wide traces, high proximity effect losses induced by the permanent-magnet field at high speed would be the consequence. As a compromise, the width of the copper traces is chosen to be 170 μm, resulting in a decreased copper filling factor. Higher copper filling factors without an increase of proximity effect losses could only be achieved when allowing smaller via-pad diameters.

Three electrical connections are needed for both coil pairs of phase A. Phase B requires two connections. Hence, for the eight connections in total, a standard eight-way 0.5-mm pitch flexible-flat-cable connector is used to connect the winding to the power amplifier and measurement circuit.

The proposed self-sensing circuit, including the measurement bridges, high frequency signal injection, demodulation, power amplifiers, and angular rotor position measurement, has been implemented on a four-layer PCB. A picture of the realized PCB which is populated with components on both sides is shown in Fig. 14. For the coupled inductors, ACM-4532 common mode chokes from TDK Inc. are used. One-nanofarad ceramic capacitors are used for C_{in} and C_m. High frequency signal injection is accomplished using a Linear Technology LTC6902 precision oscillator configured to provide two 90° phase-shifted rectangular signals with a frequency of 10 MHz. An additional operational amplifier is used as voltage follower in order to provide an injected current with an amplitude of approximately 10 mA. Demodulation is accomplished with differential signaling through a bandpass and amplifier stage, whose output signals are rectified using single-pole double-throw analog switches. An integrated low-pass filter (LT6600-2.5) eliminates the high frequency spectral components and provides a voltage signal proportional to the displacement. The damper current control and power amplification is implemented with an Analog Devices AD8397 operational amplifier providing a maximum damper current of 310 mA for each phase. The signal processing circuitry is running from a 5-V single supply; the power amplifiers are powered by a ±8-V dual supply.

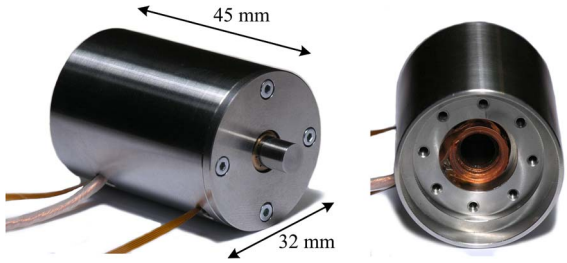

Fig. 15. High-speed electric machine prototype (250 W and 500 kr/min) with hybrid bearing system.

In a test setup, the described FPC winding is integrated into an electric machine which is designed for a power of 250 W and a target speed of up to 500 kr/min. Fig. 15 shows a picture of the electric machine with the installed FPC dampers.

The maximum allowable speed of the machine depends on the construction and material selection of the used rotor. For a rotor with a titanium grade V retaining sleeve and an encapsulated samarium–cobalt magnet, the rotor natural frequencies and material stresses due to centrifugal forces would allow for a maximum speed of 500 kr/min. For a rotor designed with stainless steel 1.4301, however, a maximum speed of approximately 400 kr/min is allowable. For first tests, a steel rotor is used because of lower wear and superior gliding properties during start and stop or in case of a bearing touchdown. The weight of the steel rotor is 16 g. The journal bearing is an eight-pad Rayleigh-step bearing with minimal clearance of nominally 8 μm and a diameter and length of 6 mm. The axial bearing is realized as a spiral grooved bearing.

The machine is operated with a Celeroton CC-75-400 pulse-amplitude-modulated inverter. At start-up, the rotor slides at first on the bearing bushings and lifts of at approximately 15 kr/min. From there, the rotor is carried by the fluid film of the gas bearing.

The displacement measurement with the FPC winding was calibrated manually by tracing the rotor along the inner surface of the bearing bushing to obtain a circle with a radius of the bearing clearance. In this static case, it was found that the directions of the measurement signal matched well with the directions of the physical displacement. In a next step, the machine was operated at low speeds where the gas bearings behave dynamically stable without the damper being active. At low speeds, only synchronous whirling motion is present which is the response of the rotor-bearing system to the synchronous excitation of the rotor imbalance. Fig. 16 shows the measured displacement output signals of the PCB prototype at a rotational speed of 22 kr/min. The synchronous whirl amplitude is around 30% of the bearing nominal clearance which corresponds to approximately 2.4 μm. It can be seen that the synchronous whirling motion is represented with high resolution; the measurement signal noise corresponds to approximately 200 nm.

In a next step, using the displacement signals, the control loop will be closed to provide a damping force and stabilize the gas bearing at higher speeds, finally up to 500 kr/min.

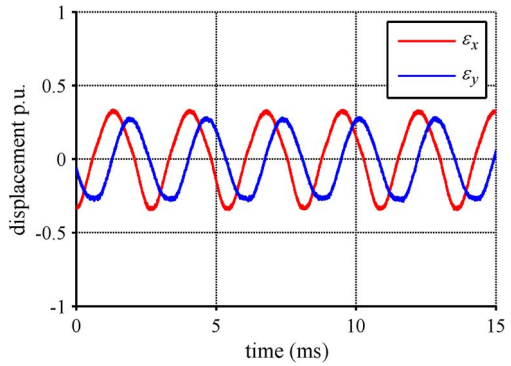

Fig. 16. Open-loop rotor displacement measurement of synchronous whirl at a speed of 22 kr/min over time. A displacement of 1 p.u. corresponds to the gas-bearing clearance (8 μm).

Hence, with the developed prototype, the expectations for a high sensitivity displacement measurement by means of the eddy-current-based self-sensing approach have been confirmed. Giving the possibility to measure rotor motion of submicrometer amplitude, the proposed self-sensing concept is considered a solid basis for vibration control of gas bearings at ultrahigh speeds.

V. Conclusion

In order to enable the use of ultrahigh-speed electrical-drive systems with high reliability and long lifetime in industrial applications, a hybrid bearing concept employing gas bearings in combination with a new small-sized self-sensing magnetic damper with auxiliary signal injection and displacement measurement electronics has been proposed. With the new approach of eddy-current-based displacement self-sensing, a method has been presented which is ideally suited for air-gap windings which are the preferred choice of winding types of ultrahigh-speed permanent-magnet machines for the targeted applications. With the self-sensing approach and with the integration of the active magnetic damper into the permanent-magnet machine, the amount of additional components, complexity, and costs is minimized. A very high sensitivity measurement has been shown with a prototype realization of the proposed concept which is expected to enable stable operation of gas bearings and permanent-magnet rotors at highest operational speeds without compromising the gas bearing's high load capacity and stiffness and allow for more generous or feasible production tolerances and, hence, lower costs.

References

[1] C. Zwyssig, J. Kolar, and S. Round, "Megaspeed drive systems: Pushing beyond 1 million r/min," *IEEE/ASME Trans. Mechatronics*, vol. 14, no. 5, pp. 564–574, Oct. 2009.

[2] D. Krahenbuhl, C. Zwyssig, and J. Kolar, "Half-controlled boost rectifier for low-power high-speed permanent-magnet generators," *IEEE Trans. Ind. Electron.*, vol. 58, no. 11, pp. 5066–5075, Nov. 2011.

[3] A. Borisavljevic, H. Polinder, and J. Ferreira, "On the speed limits of permanent-magnet machines," *IEEE Trans. Ind. Electron.*, vol. 57, no. 1, pp. 220–227, Jan. 2010.

[4] P.-D. Pfister and Y. Perriard, "Very-high-speed slotless permanent-magnet motors: Analytical modeling, optimization, design, and torque measurement methods," *IEEE Trans. Ind. Electron.*, vol. 57, no. 1, pp. 296–303, Jan. 2010.

[5] J. Luomi, C. Zwyssig, A. Looser, and J. Kolar, "Efficiency optimization of a 100-W 500 000-r/min permanent-magnet machine including air-friction losses," *IEEE Trans. Ind. Appl.*, vol. 45, no. 4, pp. 1368–1377, Jul./Aug. 2009.

[6] T. Baumgartner, R. Burkart, and J. Kolar, "Analysis and design of an ultra-high-speed slotless self-bearing permanent-magnet motor," in *Proc. 38th Annu. IEEE IECON*, Oct. 2012, pp. 4477–4483.

[7] T. Baumgartner, R. Burkart, and J. Kolar, "Analysis and design of a 300 W–500 000 rpm slotless self-bearing permanent-magnet motor," *IEEE Trans. Ind. Electron.*, to be published.

[8] J. Fang, S. Zheng, and B. Han, "AMB vibration control for structural resonance of double-gimbal control moment gyro with high-speed magnetically suspended rotor," *IEEE/ASME Trans. Mechatronics*, vol. 18, no. 1, pp. 32–43, Feb. 2013.

[9] H. Marsh, "The stability of aerodynamic gas bearings," in *Mechanical Engineering Science Monograph*. London, U.K.: Inst. Mech. Eng., Jun. 1965.

[10] D. Kim, A. M. Rimpel, S. S. Chang, and J. H. Kim, "Design and manufacturing of mesoscale tilting pad gas bearings for 100–200 W class powerMEMS applications," *ASME J. Eng. Gas Turbines Power*, vol. 131, no. 4, pp. 042503-1–042503-11, Apr. 2009.

[11] D. Flemming and B. Hamrock, "Optimization of self-acting herringbone journal bearings for maximum stability," in *Proc. 6th Int. Gas Bearing Symp.*, Mar. 1974, pp. CI–Cu.

[12] M. Salehi, H. Heshmat, J. F. Walton, and M. Tomaszewski, "Operation of a mesoscopic gas turbine simulator at speeds in excess of 700,000 rpm on foil bearings," *ASME J. Eng. Gas Turbines Power*, vol. 129, no. 1, pp. 170–176, Mar. 2004.

[13] D. Kim, M. S. Hossain, S.-J. Son, C.-J. Choi, and D. Krähenbühl, "Five millimeter air foil bearing operating at 350,000 rpm in a micro electric motor drive," in *Proc. ASME/STLE IJTC*, 2011, pp. 163–166.

[14] T. Waumans, J. Peirs, F. Al-Bender, and D. Reynaerts, "Aerodynamic journal bearing with a flexible, damped support operating at 7.2 million DN," *J. Micromech. Microeng.*, vol. 21, no. 10, p. 104014, 2011.

[15] J. Peirs, C. Zwyssig, T. Waumans, F. Al-Bender, and D. Reynaerts, "600 000 rpm electrical motor/generator supported by air bearings," in *Proc. 12th Int. Workshop Micro Nanotechnol. Power Generation Energy Convers. Appl. PowerMEMS*, Dec. 2012, pp. 165–168.

[16] A. El-Shafei and A. S. Dimitri, "Controlling journal bearing instability using active magnetic bearings," *ASME J. Eng. Gas Turbines Power*, vol. 132, no. 1, p. 012502, 2010.

[17] A. Looser and J. Kolar, "A hybrid bearing concept for high-speed applications employing aerodynamic gas-bearings and a self-sensing active magnetic damper," in *Proc. 37th Annu. IEEE IECON*, Nov. 2011, pp. 1686–1691.

[18] A. Looser, T. Baumgartner, J. Kolar, and C. Zwyssig, "Analysis and measurement of three-dimensional torque and forces for slotless permanent-magnet motors," *IEEE Trans. Ind. Appl.*, vol. 48, no. 4, pp. 1258–1266, Jul./Aug. 2012.

[19] G. Schweitzer and E. Maslen, *Magnetic Bearings—Theory, Design, and Application to Rotating Machinery*. New York, NY, USA: Springer-Verlag, 2009.

[20] J. Vohr and C. Chow, "Characteristics of herringbone-grooved, gas-lubricated journal bearings," *J. Basic Eng.*, vol. 87, no. 3, pp. 568–578, Sep. 1965.

[21] T. Kuwajima, T. Nobe, K. Ebara, A. Chiba, and T. Fukao, "An estimation of the rotor displacements of bearingless motors based on a high frequency equivalent circuits," in *Proc. 4th IEEE Int. Conf. Power Electron. Drive Syst.*, Oct. 2001, vol. 2, pp. 725–731.

[22] A. Schammass, R. Herzog, P. Buehler, and H. Bleuler, "New results for self-sensing active magnetic bearings using modulation approach," *IEEE Trans. Control Syst. Technol.*, vol. 13, no. 4, pp. 509–516, Jul. 2005.

[23] T. Tera, Y. Yamauchi, A. Chiba, T. Fukao, and M. Rahman, "Performances of bearingless and sensorless induction motor drive based on mutual inductances and rotor displacements estimation," *IEEE Trans. Ind. Electron.*, vol. 53, no. 1, pp. 187–194, Feb. 2006.

[24] R. Larsonneur and P. Buehler, "New radial sensor for active magnetic bearings," in *Proc. 9th Int. Symp. Magn. Bearings*, 2004, pp. 495–499.

[25] A. Muesing, C. Zingerli, and J. W. Kolar, "PEEC-based numerical optimization of compact radial position sensors for active magnetic bearings," in *Proc. 5th CIPS Conf.*, 2008, pp. 1–5.

[26] B. Dehez, M. Markovic, and Y. Perriard, "Analysis and comparison of classical and flex-PCB slotless windings in BLDC motors," in *Proc. IEEE 15th ICEMS*, Oct. 2012, pp. 1–6.

Andreas Looser (S'08) received the M.Sc. degree in electrical engineering, focusing on electrical-drive systems, power electronics, and very large scale integration, from ETH Zürich, Zürich, Switzerland, in 2007, where he has been working toward the Ph.D. degree with a focus on high-speed electrical drives and bearing technology in the Power Electronic Systems Laboratory since 2008.

He has also been working as a Research Associate in the Power Electronic Systems Laboratory, ETH Zurich.

Johann W. Kolar (M'89–SM'04–F'10) received the M.Sc. and Ph.D. degrees (*summa cum laude/ promotio sub auspiciis praesidentis rei publicae*) from the Vienna University of Technology, Vienna, Austria.

Since February 1, 2001, he has been a Professor and the Head of the Power Electronic Systems Laboratory, ETH Zurich, Zurich, Switzerland. He has proposed numerous novel pulse width modulation converter topologies and modulation and control concepts, e.g., the Vienna Rectifier, the Swiss Rectifier, and the Three-Phase AC–AC Sparse Matrix Converter. He has published over 550 scientific papers in international journals and conference proceedings and filed more than 110 patents.